

**A direct comparison between field-measured  
and sensor-based estimates of soil carbon  
dioxide flux across six National Ecological  
Observatory Network sites enabled by the  
neonSoilFlux R package**

John Zobitz<sup>1</sup>      Ed Ayres<sup>2</sup>      Zoey Werbin<sup>3</sup>      Ridwan Abdi<sup>1</sup>  
Natalie Ashburner-Wright<sup>4</sup>      Lillian Brown<sup>4</sup>  
Ryan Frink-Sobierajski<sup>4</sup>      Lajntxiag Lee<sup>1</sup>      Dijonë Mehmeti<sup>1</sup>  
Christina Tran<sup>4</sup>      Ly Xiong<sup>1</sup>      Naupaka Zimmerman<sup>4</sup>

<sup>1</sup> Augsburg University, 2211 Riverside Avenue, Minneapolis, MN 55454

<sup>2</sup> National Ecological Observatory Network, 1685 38th Street, Suite 100, Boulder, CO 80301

<sup>3</sup> Boston University, 5 Cummington Street, Boston, MA 02215

<sup>4</sup> University of San Francisco, 2130 Fulton Street, San Francisco, CA 94117

## 14 **Acknowledgments**

15 JZ acknowledges Kathleen O'Rourke for code development. NZ thanks technical staff at  
16 USF for support with field gear assembly and shipping. We thank the NEON field staff  
17 and assignable assets teams for facilitating each of the six NEON site visits. We are grateful  
18 to LI-COR technical staff for helpful discussions about optimal sampling methods. This work  
19 was supported by NSF DEB grant #2017829 awarded to JZ, and NSF DEB grant #2017860  
20 awarded to NZ.

## 21 **Conflict of Interest Statements**

22 None of the authors have a financial, personal, or professional conflict of interest related to  
23 this work.

## 24 **Author Contributions**

25 Conceptualization: JZ, NZ; Methodology: EA, JZ, NZ; Software: JZ, NZ, ZW, E A, DM, RA,  
26 LX, LL; Validation: JZ, NZ; Formal Analysis: JZ, NZ, DM, RA, LX, LL; Investigation: JZ,  
27 NZ, RF-S, CT, NA-W, LB; Resources: JZ, NZ; Data curation: JZ, NZ, DM, LX; Writing  
28 – original draft: JZ, NZ; Writing – review and editing: JZ, NZ, ZW, EA, CT, DM, LX,;  
29 Visualization: JZ, NZ, DM, RA, LX; Supervision: JZ; NZ; Project Administration: JZ; NZ;  
30 Funding Acquisition: JZ; NZ

## <sup>31</sup> **Data Availability**

<sup>32</sup> Data available from the Zenodo LINK <http://dx.doi.org/10.5061/dryad.41qh7> (Kiere & Drum-

<sup>33</sup> mond 2016).”

# 1 Abstract

A key component of constraining the uncertainty of the terrestrial carbon sink is quantification of terrestrial soil carbon fluxes, which vary across time and ecosystem type. One method for the estimation of these fluxes and their associated uncertainties is the flux gradient method, which can be calculated via a variety of existing approaches. Robust estimation of soil carbon fluxes on a sub-daily level requires measurements of soil CO<sub>2</sub> concentration, water content, temperature, and other environmental measurements and soil properties. These data are publicly available from the National Ecological Observatory Network at sites spanning a range of 20 different ecoclimatic domains across the continental United States, Puerto Rico, Alaska, and Hawai'i. We present an R software package (`neonSoilFlux`) that acquires NEON soil environmental data and computes soil carbon flux at a half-hourly time step at a user-specified NEON site and month in a tidy data format. To validate the computed fluxes, we visited six focal NEON sites and measured soil carbon fluxes using a closed-dynamic chamber approach. The validation confirmed that a primary challenge in reducing soil carbon flux uncertainty is correctly characterizing diffusivity and soil water content across the soil profile. Outputs from the `neonSoilFlux` package contribute to existing databases of soil carbon flux measurements, providing near real-time estimates of a critical component of the terrestrial carbon cycle.

## 1.1 Keywords

Soil carbon, carbon dioxide, flux gradient, carbon cycle, field validation, soil respiration, ecosystem variability, diffusion

## 54 2 Data for peer review

55 Anonymous data and code for peer review is available here: [LINK](#)

## 56 3 Introduction

57 Soils contain the largest reservoir of terrestrial carbon (Jobbágy & Jackson, 2000). A critical  
58 component of this reservoir is soil organic matter, the accumulation of which is influenced  
59 by biotic factors such as above-ground plant inputs (Jackson et al., 2017). These inputs in  
60 turn are influenced by environmental factors such as growing season length, temperature, and  
61 moisture (Desai et al., 2022), which also affect the breakdown of soil organic matter and its  
62 return to the atmosphere. Across heterogeneous terrestrial landscapes, the interplay between  
63 these biotic and abiotic factors influence the size of the soil contribution to the terrestrial  
64 carbon sink (Friedlingstein et al., 2023). However, the heterogeneity of these processes across  
65 diverse ecosystems in the context of rapid environmental change leads to large uncertainty in  
66 the magnitude of this sink in the future, and thus a pressing need to quantify changes in soil  
67 carbon pools and fluxes across scales.

68 Ecological observation networks such as the United States' National Ecological Observatory  
69 Network (NEON) and others (e.g. FLUXNET or the Integrated Carbon Observation System)  
70 present a significant advancement in the nearly continuous observation of biogeochemical pro-  
71 cesses at the continental scale. Notably, at 47 terrestrial sites across the continental United  
72 States, NEON provides half-hourly measurements of soil CO<sub>2</sub> concentration, temperature,  
73 and moisture at different vertical depths. Each of these NEON sites also encompasses mea-  
74 surements of the cumulative sum of all ecosystem carbon fluxes in an airshed using the eddy  
75 covariance technique (Baldocchi, 2014). Soil observations provided by NEON are on the same

timescale and standardized with eddy covariance measurements from FLUXNET. These types of nearly continuous observational data (NEON and FLUXNET) can be used to reconcile differences between model-derived or data-estimated components of ecosystem carbon flux (Jian et al., 2022; Luo et al., 2011; Phillips et al., 2017; J. Shao et al., 2015; P. Shao et al., 2013; Sihi et al., 2016).

Beyond direct observations of soil CO<sub>2</sub> concentrations and other environmental variables such as moisture or temperature, estimated or observed soil carbon fluxes are a key metric for understanding change in soil carbon pools over time (Bond-Lamberty et al., 2024). A soil carbon flux to the atmosphere ( $F_S$ , units  $\mu\text{mol m}^{-2} \text{s}^{-1}$ ), represents the aggregate process of transfer of soil CO<sub>2</sub> to the atmosphere from physical and biological processes (e.g. diffusion and respiration). Measurements of soil carbon fluxes can be coupled with empirical or process models of soil carbon. Soil carbon fluxes can be assumed to encompass soil carbon respiration from autotrophic or heterotrophic sources (Davidson et al., 2006), typically assumed to be static across the soil biome and modeled with a exponential  $Q_{10}$  paradigm (Bond-Lamberty et al., 2004; Chen & Tian, 2005; Hamdi et al., 2013).

One method by which  $F_S$  is measured in the field is through the use of soil chambers in a closed, well-mixed system (Norman et al., 1997) with headspace trace gas concentrations measured with an infrared gas analyzer (IRGA).  $F_S$  can also be estimated from soil CO<sub>2</sub> measurements at different depths in the soil using the flux-gradient method (Maier & Schack-Kirchner, 2014). This method is an approach that uses conservation of mass to calculate flux at a vertical soil depth  $z$  at steady state by applying Fick’s law of diffusion. A simplifying assumption for the flux-gradient method is that there is no mass transfer in the other spatial dimensions  $x$  and  $y$  (Maier & Schack-Kirchner, 2014). The diffusivity profile, a key component of this calculation, varies across the soil depth as a function of soil temperature, soil volumetric water content, atmospheric air pressure, and soil bulk density (Millington & Shearer, 1971; Moldrup et al.,

101 1999; Sallam et al., 1984).

102 Databases such as the Soil Respiration Database (SRDB) or the Continuous Soil Respiration  
103 Database (COSORE) add to the growing network of resources for making collected observa-  
104 tions of soil fluxes available to other workers (Bond-Lamberty, 2018; Bond-Lamberty et al.,  
105 2020; Bond-Lamberty & Thomson, 2010; Jian et al., 2021; Jiang et al., 2024). However, these  
106 databases currently encompass primarily direct soil measurements of fluxes (i.e. those using  
107 methods like the closed-chamber method described above). Currently, NEON provides all  
108 measurements to calculate  $F_S$  from Fick’s law, but soil flux as a derived data product was  
109 descoped from the initial network launch due to budget constraints (Berenbaum et al., 2015).  
110 Deriving estimates of  $F_S$  using continuous sensor data across NEON sites thus represents a  
111 high priority.

112 This study describes an R software package, **neonSoilFlux**, that can be used to derive a  
113 standardized estimate of  $F_S$  at all terrestrial NEON sites. After calculating these flux estimates,  
114 we then validated them against direct chamber-based field observations of soil carbon dioxide  
115 flux from a subset of terrestrial NEON sites spanning six states.

116 Key objectives of this study are to:

- 117 1. Apply the flux-gradient method to estimate soil CO<sub>2</sub> flux from continuous sensor mea-  
118 surements across NEON sites.
- 119 2. Benchmark estimated soil carbon fluxes against field measurements (e.g. direct measure-  
120 ments of soil flux).
- 121 3. Identify sources of error in the flux-gradient approach across diverse sites in order to  
122 guide future work.

## 123 **4 Materials and Methods**

### 124 **4.1 Field methods**

#### 125 **4.1.1 Focal NEON Sites**

126 In order to acquire field data to validate model predictions of flux, we selected six terrestrial  
127 NEON sites for analysis. We conducted field measurement campaigns at these sites, which  
128 span a range of environmental gradients and terrestrial domains (Table 1). SJER, SRER, and  
129 WREF were visited during May and June of 2022, and WOOD, KONZ, and UNDE during  
130 May and June of 2024.

131 Over the course of two field campaigns in 2022 and 2024, we conducted week-long visits at each  
132 site. In consultation with NEON field staff, we first selected a specific plot in the soil sampling  
133 array to maximize the concurrent availability of sensor data. We then made measurements of  
134 flux on an hourly or half-hourly interval for 8 hours each day after letting temporarily-installed  
135 soil collar(s) equilibrate for approximately 24 hours.



Table 1: Listing of NEON sites studied for field work and analysis.  $\overline{T_S}$ : average soil temperature during field measurements.  $\overline{SWC}$ : average soil water content during field measurements. Soil plot refers to the particular location in the soil sensor array (denoted as HOR by NEON) where field measurements were made.

Site (NEON site ID)	Location	Ecosystem type	Mean annual tempera- ture	$\overline{T_S}$ (°)	Mean annual precipita- tion	$\overline{SWC}$ (%)	Field measure- ment dates	Soil plot
Santa Rita Experi- mental Range (SRER)	31.91068, - 110.83549	Shrubland	19.3°C	47.6°	346 mm	4.0%	29 May 2024 - 01 June 2024	004
San Joaquin Experi- mental Range (SJER)	37.10878, - 119.73228	Oak woodland	16.4°C	41.7°	540 mm	1.2%	01 June 2022 - 04 June 2022	005
Wind River Experi- mental Forest (WREF)	45.82049, - 121.95191	Evergreen forest	9.2°C	15.3°	2225 mm	27.2%	07 June 2022 - 09 June 2022	001
Chase Lake National Wildlife Refuge (WOOD)	47.1282, - 99.241334	Restored prairie grassland	4.9°C	14.9°	495 mm	14.9%	03 June 2024 - 09 June 2024	001
Konza Prairie Biological Station (KONZ)	39.100774, - 96.563075	Tallgrass Prairie	12.4°C	23.4°	870 mm	23.4%	29 May 2024 - 01 June 2024	001

Table 1: Listing of NEON sites studied for field work and analysis.  $\overline{T_S}$ : average soil temperature during field measurements.  $\overline{SWC}$ : average soil water content during field measurements. Soil plot refers to the particular location in the soil sensor array (denoted as HOR by NEON) where field measurements were made.

Site (NEON site ID)	Location	Ecosystem type	Mean annual tempera- ture $\overline{T_S}$ (°)	Mean annual precipita- tion	$\overline{SWC}$ (%)	Field measure- ment dates	Soil plot
University of Notre Dame Environ- mental Research Center (UNDE)	46.23391, - 89.537254	Deciduous forest	4.3° 13.0°	802 mm	13.0%	22 May 2024 - 25 May 2024	004

#### 4.1.2 Soil collar placement

Either one (2022 sampling campaign) or two (2024 sampling campaign) PVC soil collars (FIXME: diameter) were installed in close proximity to the permanent NEON soil sensors at each site. The soil plot where measurements were taken was chosen at each site in consultation with NEON staff to maximize likelihood of quality soil sensor measurements during the duration of the IRGA measurements at each site.

IN PROGRESS: Add graphic of soil plot layout and placement of soil collar(s) – could make diagram in OmniGraffle?

### 144 **4.1.3 Infrared gas analyzer measurements of soil CO<sub>2</sub> flux**

145 During the summer 2022 field campaign, a LI-COR 6800 with soil flux chamber attachment  
146 was used to measure soil fluxes for 8 hours each day on an hourly interval. During the  
147 summer 2024 field campaign, the LI-6800 measurements were taken on a half-hourly interval  
148 and were paired with an automated soil flux chamber setup (FIXME multiplexer, IRGA,  
149 chamber model numbers) that made automated measurements on a half-hourly interval 24  
150 hours a day while we were on site. Each instrument was paired with a soil temperature  
151 and moisture probe (FIXME: Stevens model #) that was used to make soil temperature and  
152 moisture measurements concurrent with the CO<sub>2</sub> flux measurements.

153 IN PROGRESS: Dead bands, measurement duration, instrument self-testing.

### 154 **4.1.4 Post-collection processing of data**

155 IN PROGRESS: LI-COR SoilFluxPro software to assess dead band and measurement dura-  
156 tion.

## 157 **4.2 neonSoilFlux R package**

158 We developed an R package (`neonSoilFlux`; <https://CRAN.R-project.org/package=neonSoilFlux>)  
159 to compute half-hourly soil carbon fluxes and uncertainties from NEON data. The  
160 objective of the `neonSoilFlux` package is a unified workflow for soil data acquisition  
161 and analysis that supplements the existing data acquisition R package `neonUtilities`  
162 (<https://CRAN.R-project.org/package=neonUtilities>). Figure 1 outlines the basic workflow  
163 of the package.

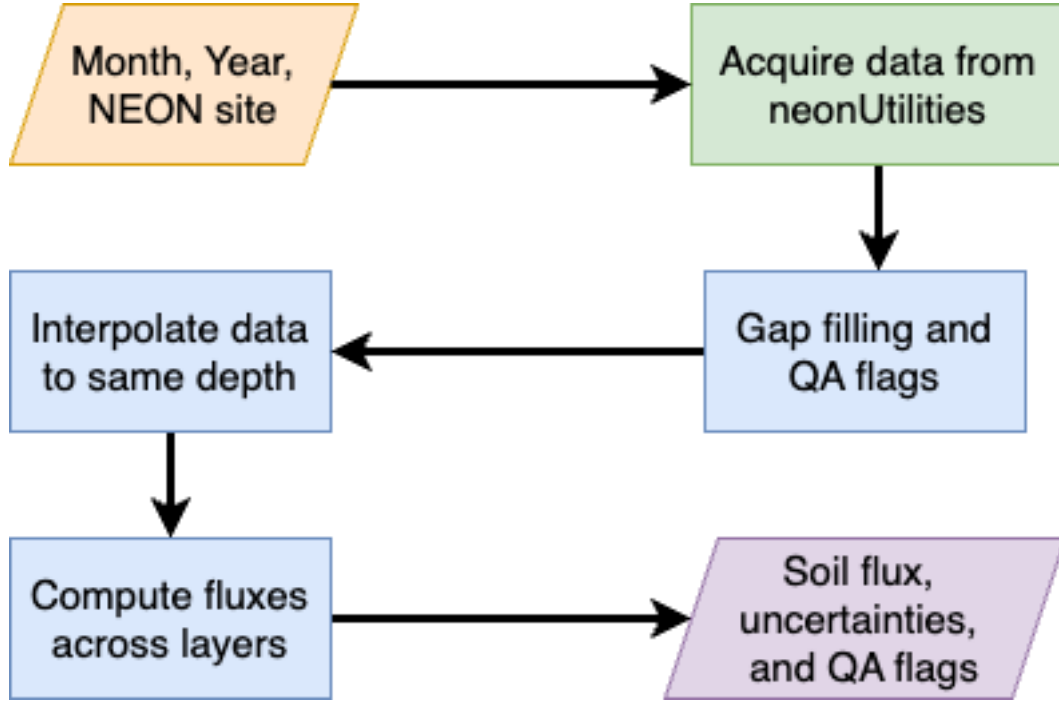


Figure 1: Diagram of `neonSoilFlux` R package. For a given month, year and NEON site (orange parallelogram), the package acquires all relevant data to compute  $F_S$  using the `neonUtilities` R package (green rectangle). Data are gap-filled according to reported QA flags and interpolated to the same measurement depth before computing the soil flux, uncertainties, and final QA flags (blue rectangles). The package reports the associated soil flux, uncertainties, and quality assurance (QA) flags for the user (purple parallelogram).

At a given NEON observation there are five replicate soil plots, each with measurements of soil CO<sub>2</sub> concentration, soil temperature, and soil moisture at different depths (Figure 2). The **neonSoilFlux** package acquires measured soil water content (National Ecological Observatory Network (NEON), 2024e), soil CO<sub>2</sub> concentration (National Ecological Observatory Network (NEON), 2024b), barometric pressure from the nearby tower (National Ecological Observatory Network (NEON), 2024a), soil temperature (National Ecological Observatory Network (NEON), 2024d), and soil properties (e.g. bulk density) (National Ecological Observatory Network (NEON), 2024c). The static soil properties were collected from a nearby soil pit during site characterization and are assumed to be constant at each site.

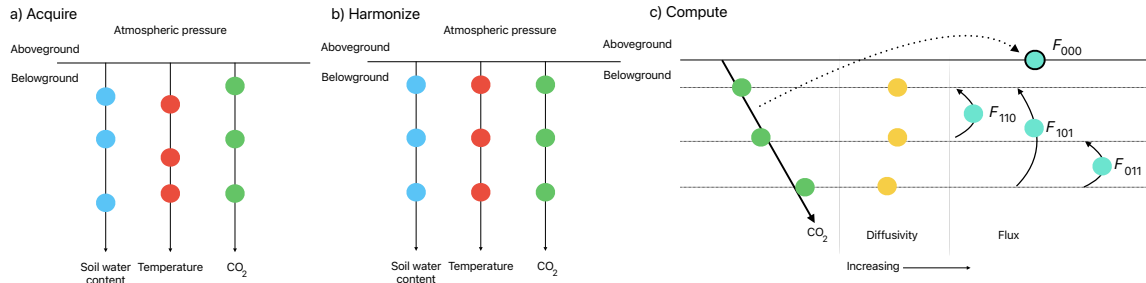


Figure 2: Model diagram for data workflow for the **neonSoilFlux** R package. a) Acquire: Data are obtained from given NEON location and horizontal sensor location, which includes soil water content, soil temperature, CO<sub>2</sub> concentration, and atmospheric pressure. All data are screened for quality assurance, with gap-filling of missing data reported. b) Any belowground data are then harmonized to the same depth as CO<sub>2</sub> concentrations using linear regression. c) The flux across a given depth is computed via Fick's law, denoted with  $F_{ijk}$ , where  $i, j$ , or  $k$  are either 0 or 1 denoting the layers the flux is computed across ( $i$  = closest to surface,  $k$  = deepest).  $F_{000}$  represents a flux estimate where the gradient  $dC/dz$  is the slope of a linear regression of CO<sub>2</sub> with depth.

The workflow to computing a value of  $F_S$  with the **neonSoilFlux** consists of three primary steps, illustrate in Figure 2. First, NEON data are acquired for a given site and month via the **neonUtilities** R package (yellow parallelogram and green rectangle in Figure 1 and Panel a in Figure 2). Acquired environmental data can be exported to a comma separated value file

177 for additional analysis. Quality assurance (QA) flags with an observation are reported as an  
178 indicator variable.

179 The next step is harmonizing the data to compute soil fluxes across soil layers. This step  
180 consists of three different actions (blue rectangles in Figure 1 and Panel b in Figure 2). If a  
181 given observation by NEON is reported as not passing a quality assurance check, we applied  
182 a gap filling method to replace that measurement with its monthly mean at that same depth  
183 (Section 4.2.1). Belowground measurements of soil water and soil temperature are then inter-  
184 polated to the same depth as soil CO<sub>2</sub> measurements. The diffusivity (Section 4.2.2) and soil  
185 flux across different soil layers (Section 4.2.3) are then computed.

186 The final step is computing a surface soil flux through extrapolation to the surface (purple  
187 parallelogram in Figure 1 and Panel c in Figure 2). Uncertainty on a soil flux measurement is  
188 computed through quadrature. An aggregate quality assurance (QA) flag for each environmen-  
189 tal measurement is also reported, representing if any gap-filled measurements were used in the  
190 computation of a soil flux. Within the soil flux-gradient method, several different approaches  
191 can be used to derive a surface flux (Maier & Schack-Kirchner, 2014); the `neonSoilFlux`  
192 package reports four different possible values of soil surface flux (Section 4.2.3).

#### 193 4.2.1 Gap-filling routine

194 NEON reports QA flags as a binary value for a given measurement and half-hourly time. We  
195 replaced any flagged measurements at a location’s spatial depth  $z$  with a bootstrapped sample  
196 of the monthly mean for all un-flagged measurements for that month. These measurements are  
197 represented by the vector  $\mathbf{m}$ , standard errors  $\sigma$ , and the 95% confidence interval (the so-called  
198 expanded uncertainty, Farrance & Frenkel (2012))  $\epsilon$ . All of these vectors have length  $M$ . We  
199 have that  $\vec{\sigma}_i \leq \vec{\epsilon}_i$ . We define the bias as  $\mathbf{b} = \sqrt{\epsilon^2 - \sigma^2}$ .

200 We generate a vector of bootstrap samples of the distribution of the monthly mean  $\bar{m}$  and  
 201 monthly standard error  $\bar{\sigma}$  the following ways:

- 202 1. Randomly sample from the uncertainty and bias independently:  $\sigma_j$  and the bias  $\mathbf{b}_k$  (not  
 203 necessarily the same sample).
- 204 2. Generate a vector  $\mathbf{n}$  of length  $N$ , where  $\mathbf{n}_i$  is a random sample from a normal distribution  
 205 with mean  $m_i$  and standard deviation  $\sigma_j$ . Since  $M < N$ , values from  $\mathbf{m}$  will be reused.
- 206 3. With these  $N$  random samples,  $\bar{y}_i = \bar{x} + \vec{b}_k$  and  $s_i$  is the sample standard deviation of  $\vec{x}$ .  
 207 We expect that  $s_i \approx \vec{\sigma}_j$ .
- 208 4. The reported monthly mean and standard deviation are then computed  $\bar{\bar{y}}$  and  $\bar{s}$ . Mea-  
 209 surements and uncertainties that did not pass the QA check are then substituted with  
 210  $\bar{\bar{y}}$  and  $\bar{s}$ .

211 This gap-filling method described here provides a consistent approach for each data stream,  
 212 however we recognize that other gap-filling alternatives may be warranted for longer-term gaps  
 213 (e.g. such as correlations with other NEON measurement levels and soil plots), or measure-  
 214 ment specific gap-filling routines. We discuss the effect of gap-filling on our measurements in  
 215 Section 6.

#### 216 4.2.2 Soil diffusivity

217 Soil diffusivity  $D_a$  at a given measurement depth is the product of the diffusivity in free air  
 218  $D_{a,0}$  ( $\text{m}^2 \text{s}^{-1}$ ) and the tortuosity  $\xi$  (no units) (Millington & Shearer, 1971).

219 We compute  $D_{a,0}$  with Equation 1:

$$D_{a,0} = 0.0000147 \cdot \left( \frac{T_i + 273.15}{293.15} \right)^{1.75} \cdot \left( \frac{P}{101.3} \right) \quad (1)$$

where  $T_i$  is soil temperature ( $^{\circ}\text{C}$ ) at depth  $i$  (National Ecological Observatory Network (NEON), 2024d) and  $P$  surface barometric pressure (kPa) (National Ecological Observatory Network (NEON), 2024a).

Previous studies by Sallam et al. (1984) and Tang et al. (2003) demonstrated the sensitivity of modeled  $F_S$  depending on the tortuosity model used to compute diffusivity. At low soil water content, the choice of tortuosity model may lead to order of magnitude differences in  $D_a$ , which in turn affect modeled  $F_S$ . The **neonSoilFlux** package uses two different models for  $\xi$ , representing the extremes reported in Sallam et al. (1984). The first approach uses the Millington-Quirk model for diffusivity, Equation 2 (Millington & Shearer, 1971):

$$\xi = \frac{(\phi - SWC_i)^{10/3}}{\phi^2} \quad (2)$$

In Equation 2,  $SWC$  is the soil water content at depth  $i$  (National Ecological Observatory Network (NEON), 2024e) and  $\phi$  is the porosity (Equation 3), which in turn is a function of soil physical properties (National Ecological Observatory Network (NEON), 2024c):

$$\phi = \left(1 - \frac{\rho_s}{\rho_m}\right) (1 - f_V) \quad (3)$$

In Equation 3,  $\rho_m$  is the particle density of mineral soil ( $2.65 \text{ g cm}^{-3}$ ),  $\rho_s$  the soil bulk density ( $\text{g cm}^{-3}$ ) excluding coarse fragments greater than 2 mm (National Ecological Observatory Network (NEON), 2024c). The term  $f_V$  is a site-specific value that accounts for the proportion of soil fragments between 2-20 mm. Soil fragments greater than 20 mm were not estimated due to limitations in the amount of soil that can be analyzed (National Ecological Observatory Network (NEON), 2024c). We assume there are no pores within rocks.



238 The second approach to calculate  $\xi$  is the Marshall model (Marshall, 1959), where  $\xi = \phi^{1.5}$ ,  
 239 with  $\phi$  defined from Equation 3.

#### 240 4.2.3 Soil flux computation

241 We applied Fick's law (Equation 4) to compute the soil flux  $F_{ij}$  ( $\mu\text{mol m}^{-2} \text{ s}^{-1}$ ) across two  
 242 soil depths  $i$  and  $j$ :

$$F_{ij} = -D_a \frac{dC}{dz} \quad (4)$$

243 where  $D_a$  is the diffusivity ( $\text{m}^2 \text{ s}^{-1}$ ) and  $\frac{dC}{dz}$  is the gradient of  $\text{CO}_2$  molar concentration  
 244 ( $\mu\text{mol m}^{-3}$ , so the gradient has units of  $\mu\text{mol m}^{-3} \text{ m}^{-1}$ ). The soil surface flux is theoretically  
 245 defined by applying Equation 4 to measurements collected at the soil surface and directly  
 246 below the surface. Measurements of soil temperature, soil water content, and soil  $\text{CO}_2$  molar  
 247 concentration across the soil profile allow for application of Equation 4 across different soil  
 248 depths. Each site had three measurement layers, so we denote the flux between which two  
 249 layers as a three-digit subscript  $F_{ijk}$  with indicator variables  $i$ ,  $j$ , and  $k$  indicate if a given  
 250 layer was used (written in order of increasing depth), according to the following:

- 251 •  $F_{000}$  is a surface flux estimate using the intercept of the linear regression of  $D_a$  with  
 252 depth and the slope from the linear regression of  $\text{CO}_2$  with depth (which represents  $\frac{dC}{dz}$   
 253 in Fick's Law). Tang et al. (2003) used this approach to compute fluxes in an oak-grass  
 254 savannah.
- 255 •  $F_{110}$ ,  $F_{011}$  are fluxes across the two most shallow layers and two deepest layers respec-  
 256 tively. The diffusivity used in Fick's Law is always at the deeper measurement layer.

When used as a surface flux estimate we assume  $\text{CO}_2$  remains constant above this flux depth.

- $F_{101}$  is a surface flux estimate using linear extrapolation using concentration measurements between the shallowest and deepest measurement layer. Hirano et al. (2003) and Tang et al. (2005) used an approach similar to  $F_{101}$  in a temperate deciduous broadleaf forest and ponderosa pine forest respectively.

Uncertainty in all  $F_{ijk}$  is computed through quadrature (Taylor, 2022).

### 4.3 Post processing evaluation

Following collection of field measurements from the LICOR and calculation of the soil fluxes from `neonSoilFlux` package, we compared measured  $F_S$  (from the LICOR instruments) to a given soil flux calculation `neonSoilFlux` for each site and flux computation method. Statistics included the associated  $R^2$  value, root mean squared error (RMSE), and signal to noise ratio (SNR), defined as the ratio of a modeled soil flux ( $F_{ijk}$ ) from `neonSoilFlux` to its quadrature uncertainty ( $\sigma_{ijk}$ ).

We observed that the range of values (e.g.  $F_{ijk} \pm \sigma_{ijk}$ ) was much larger than the measured field flux. We evaluated  $|F_S - F_{ijk}| < (1 - \epsilon)\sigma_{ijk}$ , where  $F_S$  is a measured field soil flux from the LICOR 6800 (the LICOR 8250 was used at only three sites). The parameter  $\epsilon$  was an uncertainty reduction factor to evaluate how much the quadrature uncertainty could be reduced while maintaining precision between modeled  $F_{ijk}$  and measured  $F_S$ .

Finally, for a half-hourly interval we also computed a *post hoc*  $D_a$  using the LICOR flux along with the  $\text{CO}_2$  surface gradient reported by NEON using the measurement levels closest to the surface.

## 5 Results

Figure 3 reports the timeseries of out the measured fluxes from the LICOR 6800 and 8250 compared to modeled soil fluxes from the `neonSoilFlux` R package. Figure 4 and and computed fluxes and uncertainty at each measurement site. Results are reported in local time. Positive values of the flux indicate that there is a flux moving towards the surface. For ease of clarity the fluxes at  $F_{111}$  and  $F_{000}$  are only shown in the top row (surface), followed by the fluxes at individual separate layer ( $F_{100}$ ,  $F_{010}$ ,  $F_{001}$ ). Overall, with the exception of WREF and SRER (discussed later) the computed fluxes were on the same order of magnitude and timing as the measured field fluxes.

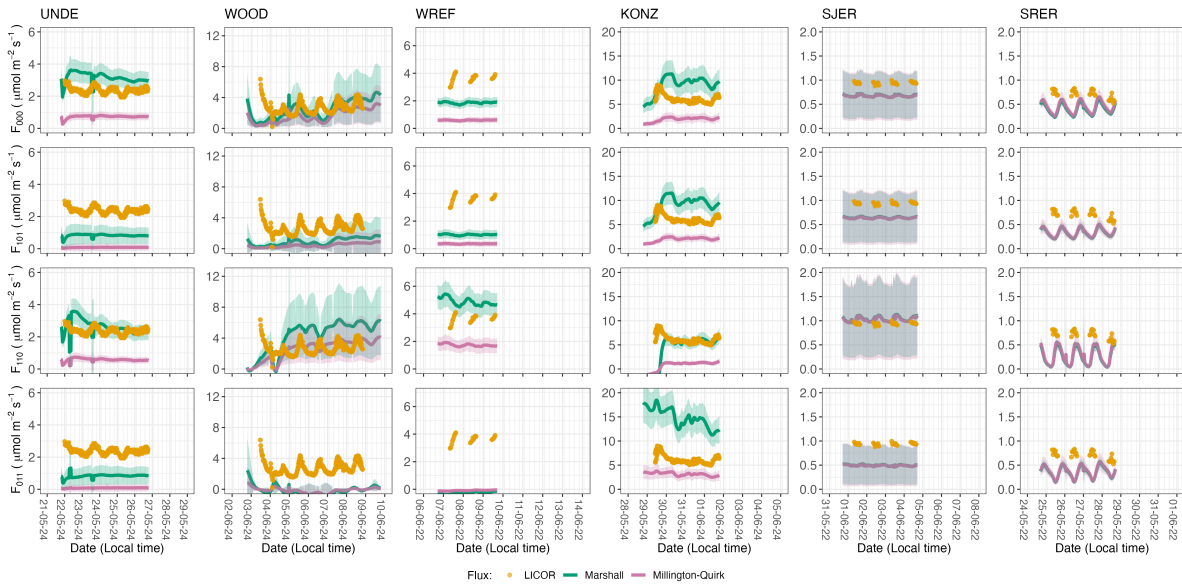


Figure 3: Timeseries of both measured  $F_S$  (yellow circles) and modeled soil fluxes (green or purple lines) by the `neonSoilFlux` R package. Fluxes from the `neonSoilFlux` R package are separated by the diffusivity model used (Millington-Quirk or Marshall, Section 4.2.2). Vertical axis labels in the first column represent the measurement levels where the flux-gradient approach is applied (Section 4.2.3). Ribbons for modeled soil fluxes represent  $\pm 1$  standard deviation. Results are reported in local time.

For a given half-hourly time period, the `neonSoilFlux` packages assigns a QA flag for a mea-

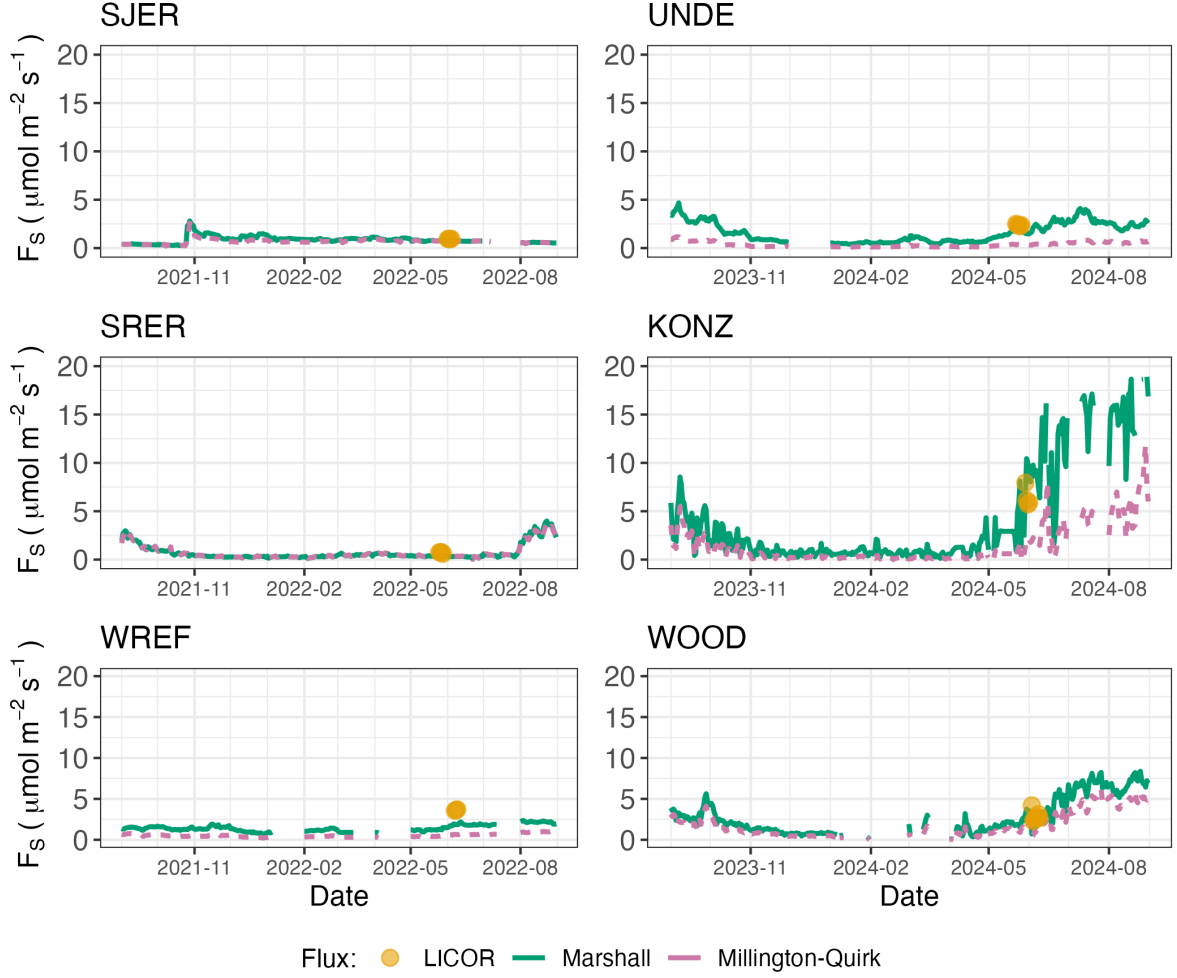


Figure 4: Timeseries of both daily-averaged field  $F_s$  (yellow circles) and daily ensemble averaged soil fluxes (green or purple lines) by the `neonSoilFlux` R package, separated by the diffusivity model used (Millington-Quirk or Marshall, Section 4.2.2). The time-series of modeled fluxes are a daily ensemble average of all flux-gradient approaches ( $F_{000}$ ,  $F_{101}$ ,  $F_{011}$ ,  $F_{110}$ , Section 4.2.3).

	Millington-Quirk		Marshall	
	NRMSE	R2	NRMSE	R2
KONZ				
$F_{110}$	0.87	0.41	0.63	0.41
$F_{101}$	0.69	0.22	0.60	0.15
$F_{011}$	0.52	0.20	1.35	0.25
$F_{000}$	0.70	0.23	0.58	0.14
SJER				
$F_{110}$	0.13	0.17	0.14	0.19
$F_{101}$	0.32	0.21	0.31	0.24
$F_{011}$	0.49	0.02	0.48	0.03
$F_{000}$	0.29	0.18	0.28	0.19
SRER				
$F_{110}$	0.56	0.00	0.59	0.00
$F_{101}$	0.66	0.53	0.67	0.52
$F_{011}$	0.69	0.49	0.70	0.49
$F_{000}$	0.58	0.51	0.61	0.51
UNDE				
$F_{110}$	0.76	0.10	0.25	0.02
$F_{101}$	0.97	0.28	0.66	0.21
$F_{011}$	0.97	0.15	0.66	0.06
$F_{000}$	0.70	0.30	0.38	0.05
WOOD				
$F_{110}$	0.44	0.03	0.93	0.02
$F_{101}$	0.89	0.07	0.74	0.05
$F_{011}$	1.12	0.02	1.22	0.01
$F_{000}$	0.56	0.06	0.46	0.05
WREF				
$F_{110}$	0.53	0.78	0.35	0.75
$F_{101}$	0.91	0.24	0.73	0.35
$F_{011}$	1.03	0.37	1.07	0.37
$F_{000}$	0.84	0.00	0.49	0.05

Figure 5

surement if more one values across all measurement depths uses gap-filled data (Section 4.2.1). Panel a of Figure 6 reports the distribution for all input environmental measurements at each site when field measurements were made. Soil fluxes are computed from 4 different types of input measurements ( $T_S$ ,  $SWC$ ,  $P$ , and  $CO_2$ ), any of which could have a QA flag in a half-hourly interval. Panel b of Figure 6 displays at each site the distribution of the number of different gap-filled measurements used to compute a half-hourly flux. The largest contribution to gap-filled measurements was soil water. SJER and WOOD utilized the largest number of gap-filled measurements, which were primarily  $SWC$  and  $T_S$ .

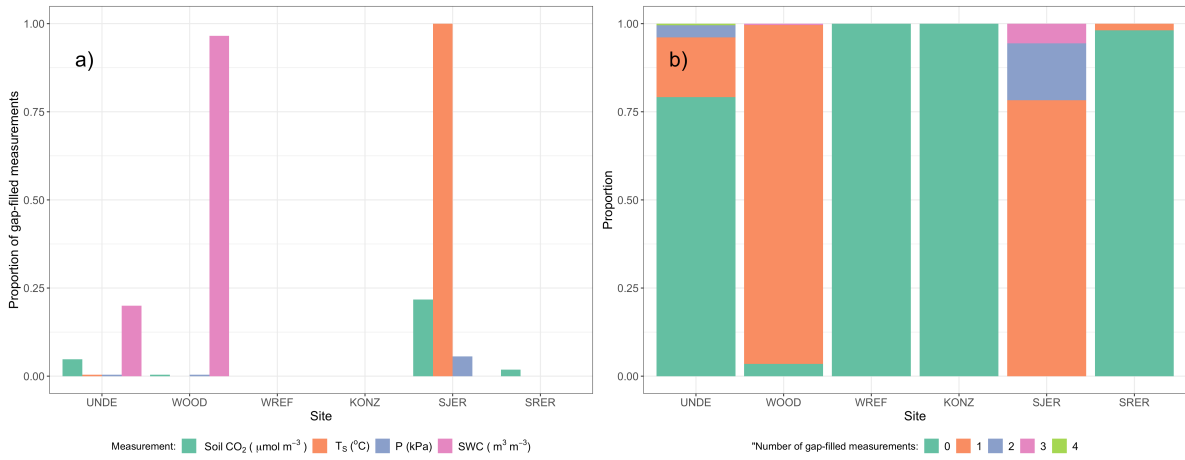


Figure 6: Panel a) Proportion of input gap-filled environmental measurements used to generate  $F_S$  from the `neonSoilFlux` package, by study site. Panel b) distribution of the usage of gap-filled measurements at each site.

Figure 7 reports both the computed SNR and the proportion of measured field fluxes within the modeled uncertainty for a given flux computation method  $F_{ijk}$  (Section 4.3). Here, values of SNR greater than unity indicates a reported uncertainty is smaller, propagated by quadrature from a relatively higher precision from measured input variables ( $CO_2$ ,  $T_S$ ,  $SWC$ , or  $P$ ). The sensitivity to the uncertainty reduction factor ( $\epsilon$ , bottom panels in Figure 7) demonstrates how accuracy could be improved if modeled uncertainty  $\sigma_{ijk}$  decreases.

Figure 8 reports the distribution of  $D_a$  (from both the Marshall and Millington-Quirk methods,

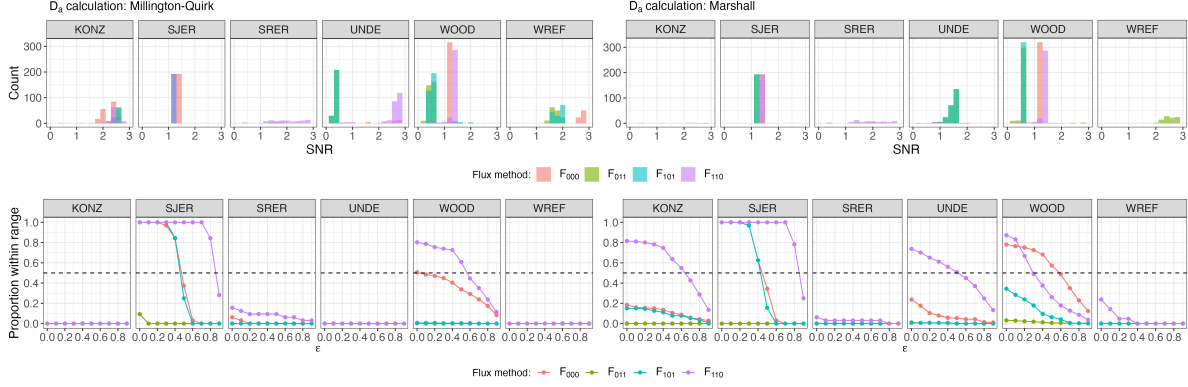


Figure 7: Top panels: distribution of SNR values across each of the different sites for modeled effluxes from the `neonSoilFlux` package, depending on the diffusivity calculation used (Millington-Quirk or Marshall, Section 4.2.2). Bottom panels: Proportion of measured  $F_S$  within the modeled range of a flux computation method  $F_{ijk}$  given an uncertainty reduction factor  $\epsilon$ , or  $|F_S - F_{ijk}| < (1 - \epsilon)\sigma_{ijk}$ .

Section 4.2.2) at each study site, and the *post hoc* computation of  $D_a$  (Section 4.2.2).

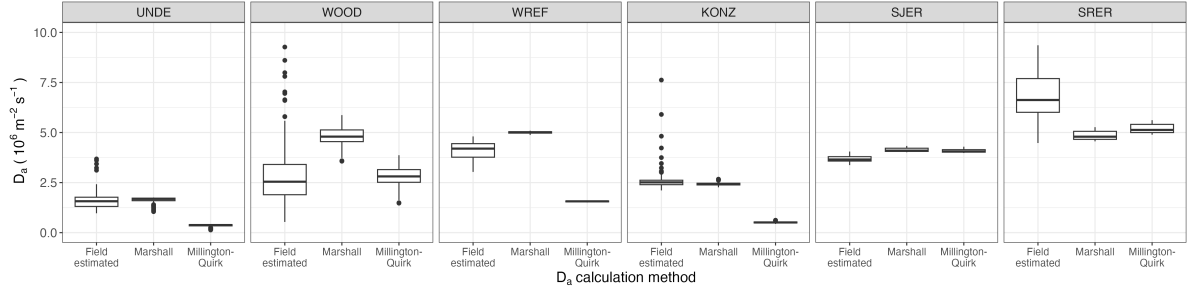


Figure 8

## 6 Discussion

This study presents a unified data science workflow to efficiently process automated measurements of belowground soil  $\text{CO}_2$  concentrations, water, and temperature to infer estimates of soil surface  $\text{CO}_2$  effluxes through application of Fick's Law (Equation 4). Our core goals in this study were: (1) to generate estimates of soil flux from continuous soil sensor data at terrestrial

NEON sites using the flux-gradient method and then (2) to compare those estimates to field-measured fluxes based on the closed chamber approach at six NEON focal sites. We discuss our progress toward these core goals through (1) an overall evaluation of the flux-gradient approach (and uncertainty calculation) and (2) site-specific evaluation of differences in estimated vs measured fluxes.

## 6.1 General evaluation of flux-gradient approach

Key assumptions of the flux-gradient approach are that  $\text{CO}_2$  concentrations increase throughout the soil profile. We found that this condition was met at XXX% across the study period. Periods where this gradient condition are not met generally are connected to biophysical processes such soil wetting events (e.g. KONZ), which have the effect of reducing the soil respiration or efflux due to a temporary reduction in diffusivity. When modeling soil respiration, typically a non-linear response function that also considers soil type is used (Bouma & Bryla, 2000; Yan et al., 2016, 2018). For the `neonSoilFlux` package, soil type is connected to the bulk density, which was characterized at each NEON site based on replicate samples collected from the site megapit at a subset of soil horizons, with an estimated uncertainty of  $\pm 5\%$  (see NEON User Guide to Soil physical and chemical properties, Megapit (DP1.00096.001)). Coarse fragment estimates also have very large uncertainties, but because the volume fraction tends to be low in surface soils it probably wouldn't contribute much additional flux uncertainty.

The largest source of uncertainty to improve reliability of the flux estimate is to prevent the usage of gap-filled data. Three sites (KONZ, SRER, and KONZ) had more than 75% of half-hourly periods with no-gap filled measurements. Two sites (SJER and WOOD) had more than 75% of half-hourly intervals with just one gap-filled measurement. While WREF reported no gap-filled measurements, field data collection occurred following a once-in-a century rainstorm with soils observed at their water holding capacity. We recommend that whenever



334 available, local field knowledge is supplementary to any QA filtering protocol of fluxes from  
335 the `neonSoilFlux` package.

336 We recognize that this gap-filling approach may lead to gap-filled values that are quite different  
337 from the actual values, such as an underestimate of soil moisture following rain events. Further  
338 extensions of the gap filling method could use more sophisticated gap-filling routines, similar to  
339 what is used for net ecosystem carbon exchange (Falge et al., 2001; Liu et al., 2023; Mariethoz  
340 et al., 2015; Moffat et al., 2007; Zhang et al., 2023). The current gap-filling routine provides  
341 a consistent approach that can be applied to each data stream, but further work may explore  
342 alternative gap-filling approaches.

343 Based on this approach, we would *a priori* expect  $F_{011} \leq F_{101} \leq F_{110} \leq F_{000}$  because the  
344 previous flux estimates ones correspond to deeper depths which will could miss  $\text{CO}_2$  produced  
345 in shallower layers. Additionally, field flux measurements should correlate with  $F_{000}$  because  
346 they represent surface fluxes.

## 347 **6.2 Evaluation of flux-gradient approach at each site**

348 Derived results from the `neonSoilFlux` package have patterns that are consistent, and  
349 comparable, to those directly measured to the field (Figure XXX). The advantage to the  
350 `neonSoilFlux` package is the calculation of fluxes across different measurement depths,  
351 allowing for additional site-specific customization. Here application of the flux-gradient  
352 method provides a baseline estimate of soil fluxes that could be complemented through  
353 additional field measurements (e.g. LICOR).

354 The six sites studied provide separate case studies for considerations when applying the flux-  
355 gradient method to evaluate resulting uncertainties and fluxes For example, SRER is charac-  
356 terized by sandy soil, which also led to the highest observed field soil temperatures. At SRER

the flux across the top two layers ( $F_{110}$ ) produced a pattern of soil flux consistent with the observed field data. The remaining methods  $F_{101}$ ,  $F_{011}$ , or  $F_{000}$  are derived from information at the deeper layer, which is decoupled both in terms of temperature and  $\text{CO}_2$  concentration.

In addition, KONZ is a site that experienced a significant rain event prior to sampling with eventual drying out over the course of the experiment. In this case we observed storage of soil water which increased the soil  $\text{CO}_2$  at the top layer, leading to negative values of flux at the start of the experiment, with the fluxes drying out afterwards. In this case only when the soil dried out (or returned to a baseline level), that the fluxes at the provided layer would work out in this case.

When considering systematic deployment of this method across a measurement network, we faced a number of independent challenges for consideration.

Figure 7 illustrates the tradeoff between accuracy for modeled fluxes (defined here as closeness to field-measured  $F_S$ ) and precision defined by the SNR, and how this is confounded by the choice of diffusivity model used. MORE HERE

Diffusivity discussion

In developing and validating our approach, we faced a number of challenges related to data availability, including... gap filling, sensor calibration, depth interpolation, rainstorms, etc These errors are all

### 6.3 Recommendations for future method development

The `neonSoilFlux` package provides three different approaches of values for a soil flux. We believe these approaches reflect a variety of site-specific determination and assumptions used to generate a soil flux measurement (Maier & Schack-Kirchner, 2014), with the choice of

method having a determinative approach on reported values. Reported results could further be distilled down using ensemble averaging approaches (Elshall et al., 2018; Raftery et al., 2005).

Figures XXX suggests that the provided uncertainty from `neonSoilFlux` is an overestimate compared to what is actually computed. When  $\epsilon = 0$  in Figure Figure 7, that means we are just using the reported uncertainty from `neonSoilFlux`. Looking at that (epsilon = 0) shows field measurements UNDE, KONZ, SJER are 100% within the reported intervals from `neonSoilFlux`. But those sites tend to have a  $\text{SNR} < 1$ , so the uncertainty is pretty noisy. For UNDE, we could even reduce the uncertainty by a factor of 75% (epsilon = 0.75), more than half of the field measurements will still be within the reported intervals. For KONZ, we are still within 70% of the reported intervals when uncertainty is reduced by 90%. That suggests that while the reported accuracy (as compared to field measurements), we do have higher precision.

These challenges notwithstanding, the method used here and made available in the `neonSoilFlux` R package has the potential to produce nearly continuous estimates of flux across all terrestrial NEON sites. These estimates are a significant improvement on available approaches to constrain the portion of ecosystem respiration attributable to the soil. This, in turn, aids in our ability to understand the components of net ecosystem flux assessed at these sites using the co-located eddy flux towers.

- Refine estimates to provide a realistic constraint on surface concentration measurements, thereby increasing the gradient.
- Apply machine learning algorithms (e.g. random trees) or model averaging techniques to generate a single flux estimate across each sites spatial location
- Benchmarking flux results to estimates provided by Net ecosystem carbon exchange.

## 7 Conclusions

We have here presented an R package `neonSoilFlux` for the estimation of soil CO<sub>2</sub> fluxes from continuous buried soil sensor measurements across terrestrial National Ecological Observatory Network sites. We compared the predicted fluxes to those measured directly using a field-based closed chamber approach. We find that...

Baldocchi, D. (2014). Measuring fluxes of trace gases and energy between ecosystems and the atmosphere - the state and future of the eddy covariance method. *Global Change Biology*, 20(12), 3600–3609. <https://doi.org/10.1111/gcb.12649>

Berenbaum, M. R., Carpenter, S. R., Hampton, S. E., Running, S. W., & Stanzione, D. C. (2015). *Report from the NSF BIO Advisory Committee Subcommittee on NEON Scope Impacts*.

Bond-Lamberty, B. (2018). New Techniques and Data for Understanding the Global Soil Respiration Flux. *Earth's Future*, 6(9), 1176–1180. <https://doi.org/10.1029/2018EF000866>

Bond-Lamberty, B., Ballantyne, A., Berryman, E., Fluet-Chouinard, E., Jian, J., Morris, K. A., Rey, A., & Vargas, R. (2024). Twenty Years of Progress, Challenges, and Opportunities in Measuring and Understanding Soil Respiration. *Journal of Geophysical Research: Biogeosciences*, 129(2), e2023JG007637. <https://doi.org/10.1029/2023JG007637>

Bond-Lamberty, B., Christianson, D. S., Malhotra, A., Pennington, S. C., Sihi, D., AghaKouchak, A., Anjileli, H., Altaf Arain, M., Armesto, J. J., Ashraf, S., Ataka, M., Baldocchi, D., Andrew Black, T., Buchmann, N., Carbone, M. S., Chang, S.-C., Crill, P., Curtis, P. S., Davidson, E. A., ... Zou, J. (2020). COSORE: A community database for continuous soil respiration and other soil-atmosphere greenhouse gas flux data. *Global Change Biology*, 26(12), 7268–7283. <https://doi.org/10.1111/gcb.15353>

Bond-Lamberty, B., & Thomson, A. (2010). A global database of soil respiration data. *Biogeosciences*, 7(6), 1915–1926. <https://doi.org/10.5194/bg-7-1915-2010>

- 428 Bond-Lamberty, B., Wang, C., & Gower, S. T. (2004). A global relationship between the  
429 heterotrophic and autotrophic components of soil respiration? *Global Change Biology*,  
430 10(10), 1756–1766. <https://doi.org/10.1111/j.1365-2486.2004.00816.x>
- 431 Bouma, T. J., & Bryla, D. R. (2000). On the assessment of root and soil respiration for soils  
432 of different textures: Interactions with soil moisture contents and soil CO<sub>2</sub> concentrations.  
433 *Plant and Soil*, 227(1), 215–221. <https://doi.org/10.1023/A:1026502414977>
- 434 Chen, H., & Tian, H.-Q. (2005). Does a General Temperature-Dependent Q<sub>10</sub> Model of Soil  
435 Respiration Exist at Biome and Global Scale? *Journal of Integrative Plant Biology*, 47(11),  
436 1288–1302. <https://doi.org/10.1111/j.1744-7909.2005.00211.x>
- 437 Davidson, E. A., Janssens, I. A., & Luo, Y. (2006). On the variability of respiration in  
438 terrestrial ecosystems: Moving beyond Q<sub>10</sub>. *Global Change Biology*, 12, 154–164. <https://doi.org/10.1111/j.1365-2486.2005.01065.x>
- 439 Desai, A. R., Murphy, B. A., Wiesner, S., Thom, J., Butterworth, B. J., Koupaie-Abyazani, N.,  
440 Muttaqin, A., Paleri, S., Talib, A., Turner, J., Mineau, J., Merrelli, A., Stoy, P., & Davis,  
441 K. (2022). Drivers of Decadal Carbon Fluxes Across Temperate Ecosystems. *Journal of*  
442 *Geophysical Research: Biogeosciences*, 127(12), e2022JG007014. [https://doi.org/10.1029/](https://doi.org/10.1029/2022JG007014)  
443 [2022JG007014](https://doi.org/10.1029/2022JG007014)
- 444 Elshall, A. S., Ye, M., Pei, Y., Zhang, F., Niu, G.-Y., & Barron-Gafford, G. A. (2018). Relative  
445 model score: A scoring rule for evaluating ensemble simulations with application to micro-  
446 bial soil respiration modeling. *Stochastic Environmental Research and Risk Assessment*,  
447 32(10), 2809–2819. <https://doi.org/10.1007/s00477-018-1592-3>
- 448 Falge, E., Baldocchi, D., Olson, R., Anthoni, P., Aubinet, M., Bernhofer, C., Burba, G.,  
449 Ceulemans, R., Clement, R., Dolman, H., Granier, A., Gross, P., Grünwald, T., Hollinger,  
450 D., Jensen, N.-O., Katul, G., Keronen, P., Kowalski, A., Lai, C. T., ... Wofsy, S. (2001).  
451 Gap filling strategies for defensible annual sums of net ecosystem exchange. *Agricultural*  
452 *and Forest Meteorology*, 107(1), 43–69. [https://doi.org/10.1016/S0168-1923\(00\)00225-2](https://doi.org/10.1016/S0168-1923(00)00225-2)
- 453

- 454 Farrance, I., & Frenkel, R. (2012). [Uncertainty of Measurement: A Review of the Rules](#)  
455 [for Calculating Uncertainty Components through Functional Relationships](#). *The Clinical*  
456 *Biochemist Reviews*, 33(2), 49–75.
- 457 Friedlingstein, P., O’Sullivan, M., Jones, M. W., Andrew, R. M., Bakker, D. C. E., Hauck,  
458 J., Landschützer, P., Le Quéré, C., Luijkx, I. T., Peters, G. P., Peters, W., Pongratz, J.,  
459 Schwingshackl, C., Sitch, S., Canadell, J. G., Ciais, P., Jackson, R. B., Alin, S. R., Anthoni,  
460 P., ... Zheng, B. (2023). Global Carbon Budget 2023. *Earth System Science Data*, 15(12),  
461 5301–5369. <https://doi.org/10.5194/essd-15-5301-2023>
- 462 Hamdi, S., Moyano, F., Sall, S., Bernoux, M., & Chevallier, T. (2013). Synthesis analysis  
463 of the temperature sensitivity of soil respiration from laboratory studies in relation to  
464 incubation methods and soil conditions. *Soil Biology and Biochemistry*, 58, 115–126. <https://doi.org/10.1016/j.soilbio.2012.11.012>
- 465
- 466 Hirano, T., Kim, H., & Tanaka, Y. (2003). Long-term half-hourly measurement of soil CO<sub>2</sub>  
467 concentration and soil respiration in a temperate deciduous forest. *Journal of Geophysical*  
468 *Research: Atmospheres*, 108(D20). <https://doi.org/10.1029/2003JD003766>
- 469 Jackson, R. B., Lajtha, K., Crow, S. E., Hugelius, G., Kramer, M. G., & Piñeiro, G. (2017).  
470 The Ecology of Soil Carbon: Pools, Vulnerabilities, and Biotic and Abiotic Controls.  
471 *Annual Review of Ecology, Evolution and Systematics*, 48(Volume 48, 2017), 419–445.  
472 <https://doi.org/10.1146/annurev-ecolsys-112414-054234>
- 473 Jian, J., Bailey, V., Dorheim, K., Konings, A. G., Hao, D., Shiklomanov, A. N., Snyder, A.,  
474 Steele, M., Teramoto, M., Vargas, R., & Bond-Lamberty, B. (2022). Historically incon-  
475 sistent productivity and respiration fluxes in the global terrestrial carbon cycle. *Nature*  
476 *Communications*, 13(1), 1733. <https://doi.org/10.1038/s41467-022-29391-5>
- 477 Jian, J., Vargas, R., Anderson-Teixeira, K., Stell, E., Herrmann, V., Horn, M., Kholod, N.,  
478 Manzon, J., Marchesi, R., Paredes, D., & Bond-Lamberty, B. (2021). A restructured and  
479 updated global soil respiration database (SRDB-V5). *Earth System Science Data*, 13(2),

255–267. <https://doi.org/10.5194/essd-13-255-2021>

Jiang, J., Feng, L., Hu, J., Liu, H., Zhu, C., Chen, B., & Chen, T. (2024). Global soil respiration predictions with associated uncertainties from different spatio-temporal data subsets. *Ecological Informatics*, 82, 102777. <https://doi.org/10.1016/j.ecoinf.2024.102777>

Jobbágy, E. G., & Jackson, R. B. (2000). The Vertical Distribution of Soil Organic Carbon and its Relation to Climate and Vegetation. *Ecological Applications*, 10(2), 423–436. [https://doi.org/10.1890/1051-0761\(2000\)010%5B0423:TVDOSO%5D2.0.CO;2](https://doi.org/10.1890/1051-0761(2000)010%5B0423:TVDOSO%5D2.0.CO;2)

Liu, K., Li, X., Wang, S., & Zhang, H. (2023). A robust gap-filling approach for European Space Agency Climate Change Initiative (ESA CCI) soil moisture integrating satellite observations, model-driven knowledge, and spatiotemporal machine learning. *Hydrology and Earth System Sciences*, 27(2), 577–598. <https://doi.org/10.5194/hess-27-577-2023>

Luo, Y., Ogle, K., Tucker, C., Fei, S., Gao, C., LaDeau, S., Clark, J. S., & Schimel, D. S. (2011). Ecological forecasting and data assimilation in a data-rich era. *Ecological Applications*, 21(5), 1429–1442. <https://doi.org/10.1890/09-1275.1>

Maier, M., & Schack-Kirchner, H. (2014). Using the gradient method to determine soil gas flux: A review. *Agricultural and Forest Meteorology*, 192–193, 78–95. <https://doi.org/10.1016/j.agrformet.2014.03.006>

Mariethoz, G., Linde, N., Jougnot, D., & Rezaee, H. (2015). Feature-preserving interpolation and filtering of environmental time series. *Environmental Modelling & Software*, 72, 71–76. <https://doi.org/10.1016/j.envsoft.2015.07.001>

Marshall, T. J. (1959). The Diffusion of Gases Through Porous Media. *Journal of Soil Science*, 10(1), 79–82. <https://doi.org/10.1111/j.1365-2389.1959.tb00667.x>

Millington, R. J., & Shearer, R. C. (1971). Diffusion in aggregated porous media. *Soil Science*, 111(6), 372–378.

Moffat, A. M., Papale, D., Reichstein, M., Hollinger, D. Y., Richardson, A. D., Barr, A. G., Beckstein, C., Braswell, B. H., Churkina, G., Desai, A. R., Falge, E., Gove, J. H., Heimann,

506 M., Hui, D., Jarvis, A. J., Kattge, J., Noormets, A., & Stauch, V. J. (2007). Comprehensive  
507 comparison of gap-filling techniques for eddy covariance net carbon fluxes. *Agricultural and*  
508 *Forest Meteorology*, 147(3), 209–232. <https://doi.org/10.1016/j.agrformet.2007.08.011>

509 Moldrup, P., Olesen, T., Yamaguchi, T., Schjønning, P., & Rolston, D. E. (1999). Modeling  
510 diffusion and reaction in soils: 9. The Buckingham-Burdine-Campbell equation for gas  
511 diffusivity in undisturbed soil. *Soil Science*, 164(2), 75.

512 National Ecological Observatory Network (NEON). (2024a). *Barometric pressure*  
513 *(DP1.00004.001)*. National Ecological Observatory Network (NEON). [https://doi.](https://doi.org/10.48443/RT4V-KZ04)  
514 [org/10.48443/RT4V-KZ04](https://doi.org/10.48443/RT4V-KZ04)

515 National Ecological Observatory Network (NEON). (2024b). *Soil CO2 concentra-*  
516 *tion (DP1.00095.001)*. National Ecological Observatory Network (NEON). [https:](https://doi.org/10.48443/E7GR-6G94)  
517 [//doi.org/10.48443/E7GR-6G94](https://doi.org/10.48443/E7GR-6G94)

518 National Ecological Observatory Network (NEON). (2024c). *Soil physical and chemical proper-*  
519 *ties, Megapit (DP1.00096.001)*. National Ecological Observatory Network (NEON). [https:](https://doi.org/10.48443/S6ND-Q840)  
520 [//doi.org/10.48443/S6ND-Q840](https://doi.org/10.48443/S6ND-Q840)

521 National Ecological Observatory Network (NEON). (2024d). *Soil temperature (DP1.00041.001)*.  
522 National Ecological Observatory Network (NEON). <https://doi.org/10.48443/Q24X-PW21>

523 National Ecological Observatory Network (NEON). (2024e). *Soil water content and water*  
524 *salinity (DP1.00094.001)*. National Ecological Observatory Network (NEON). [https://doi.](https://doi.org/10.48443/A8VY-Y813)  
525 [org/10.48443/A8VY-Y813](https://doi.org/10.48443/A8VY-Y813)

526 Norman, J. M., Kucharik, C. J., Gower, S. T., Baldocchi, D. D., Crill, P. M., Rayment, M.,  
527 Savage, K., & Striegl, R. G. (1997). A comparison of six methods for measuring soil-  
528 surface carbon dioxide fluxes. *Journal of Geophysical Research: Atmospheres*, 102(D24),  
529 28771–28777. <https://doi.org/10.1029/97JD01440>

530 Phillips, C. L., Bond-Lamberty, B., Desai, A. R., Lavoie, M., Risk, D., Tang, J., Todd-Brown,  
531 K., & Vargas, R. (2017). The value of soil respiration measurements for interpreting and



532 modeling terrestrial carbon cycling. *Plant and Soil*, 413(1), 1–25. <https://doi.org/10.1007/s11104-016-3084-x>

533

534 Raftery, A. E., Gneiting, T., Balabdaoui, F., & Polakowski, M. (2005). *Using Bayesian Model*

535 *Averaging to Calibrate Forecast Ensembles*. <https://doi.org/10.1175/MWR2906.1>

536 Sallam, A., Jury, W. A., & Letey, J. (1984). Measurement of Gas Diffusion Coefficient under

537 Relatively Low Air-filled Porosity. *Soil Science Society of America Journal*, 48(1), 3–6.

538 <https://doi.org/10.2136/sssaj1984.03615995004800010001x>

539 Shao, J., Zhou, X., Luo, Y., Li, B., Aurela, M., Billesbach, D., Blanken, P. D., Bracho, R.,

540 Chen, J., Fischer, M., Fu, Y., Gu, L., Han, S., He, Y., Kolb, T., Li, Y., Nagy, Z., Niu, S.,

541 Oechel, W. C., ... Zhang, J. (2015). Biotic and climatic controls on interannual variability

542 in carbon fluxes across terrestrial ecosystems. *Agricultural and Forest Meteorology*, 205,

543 11–22. <https://doi.org/10.1016/j.agrformet.2015.02.007>

544 Shao, P., Zeng, X., Moore, D. J. P., & Zeng, X. (2013). Soil microbial respiration from

545 observations and Earth System Models. *Environmental Research Letters*, 8(3), 034034.

546 <https://doi.org/10.1088/1748-9326/8/3/034034>

547 Sihi, D., Gerber, S., Inglett, P. W., & Inglett, K. S. (2016). Comparing models of microbial–

548 substrate interactions and their response to warming. *Biogeosciences*, 13(6), 1733–1752.

549 <https://doi.org/10.5194/bg-13-1733-2016>

550 Tang, J., Baldocchi, D. D., Qi, Y., & Xu, L. (2003). Assessing soil CO<sub>2</sub> efflux using continuous

551 measurements of CO<sub>2</sub> profiles in soils with small solid-state sensors. *Agricultural and Forest*

552 *Meteorology*, 118(3), 207–220. [https://doi.org/10.1016/S0168-1923\(03\)00112-6](https://doi.org/10.1016/S0168-1923(03)00112-6)

553 Tang, J., Misson, L., Gershenson, A., Cheng, W., & Goldstein, A. H. (2005). Continuous

554 measurements of soil respiration with and without roots in a ponderosa pine plantation

555 in the Sierra Nevada Mountains. *Agricultural and Forest Meteorology*, 132(3), 212–227.

556 <https://doi.org/10.1016/j.agrformet.2005.07.011>

557 Taylor, J. R. (2022). *An Introduction to Error Analysis: The Study of Uncertainties in Physical*

558      *Measurements, Third Edition* (3rd ed.). University Science Press.

559    Yan, Z., Bond-Lamberty, B., Todd-Brown, K. E., Bailey, V. L., Li, S., Liu, C., & Liu, C. (2018).

560      A moisture function of soil heterotrophic respiration that incorporates microscale processes.

561      *Nature Communications*, 9(1), 2562. <https://doi.org/10.1038/s41467-018-04971-6>

562    Yan, Z., Liu, C., Todd-Brown, K. E., Liu, Y., Bond-Lamberty, B., & Bailey, V. L. (2016).

563      Pore-scale investigation on the response of heterotrophic respiration to moisture conditions

564      in heterogeneous soils. *Biogeochemistry*, 131(1), 121–134. [https://doi.org/10.1007/s10533-](https://doi.org/10.1007/s10533-016-0270-0)

565      [016-0270-0](https://doi.org/10.1007/s10533-016-0270-0)

566    Zhang, R., Kim, S., Kim, H., Fang, B., Sharma, A., & Lakshmi, V. (2023). Temporal

567      Gap-Filling of 12-Hourly SMAP Soil Moisture Over the CONUS Using Water Balance

568      Budgeting. *Water Resources Research*, 59(12), e2023WR034457. [https://doi.org/10.1029/](https://doi.org/10.1029/2023WR034457)

569      [2023WR034457](https://doi.org/10.1029/2023WR034457)